CONCEPT OF A VARIABLE CHORD-EXTENSION

Christoph Balzarek, christoph.balzarek@dlr.de, German Aerospace Center (DLR) Institute of Composite Structures and Adaptive Systems, Lilienthalplatz 7 38108 Braunschweig Germany

Johannes Riemenschneider, johannes.riemenschneider@dlr.de, German Aerospace Center (DLR) Institute of Composite Structures and Adaptive Systems, Lilienthalplatz 7 38108 Braunschweig, Germany

Rohin Kumar Majeti, Rohin.Majeti@dlr.de, German Aerospace Center (DLR) Institute of Flight Systems, Lilienthalplatz 7 38108 Braunschweig, Germany

Abstract

Among all kinds of aircraft, helicopters are standing out due to their capability for both forward flight and hovering. This range of flight conditions requires a special blade design, resulting in a rotor blade geometry, which represents a compromise between the different flight conditions. Morphing rotor blades could address this issue, by changing the rotor blade shape according to the demands of the current flight state. From rotor dynamic calculations it is known, that longer chord length at the blade root and increased pre-twist would increase the performance in hover [1,3], whereas shorter chord and less twist are beneficial for fast forward flight.

Based on this assumption, a structural concept has been worked out for a blade design with a variable chord length in the rotor root region. The model, which belongs to that concept forms the basis of a performance calculation.

The structural concept consists of a pivot point at around 60% R and the chord extension is linearly increasing all the way to the blade root at 22% R. In this region an auxiliary spar is dividing the blade into a conventional rigid front part and a morphing rear part, whose structural design is the main focus of this paper. It consists of two components: a flexible skin made of rubber-like EPDM material, which is reinforced in the spanwise direction by fibers, as well as an inner support structure.

The design drivers for the skin thickness are shape accuracy on one end and actuator force to extend the mechanism and stretch the skin on the other end. The underlying support structure consists of vertical GFRP extending in span wise direction. Design parameters for those webs are the distance between webs, which relates to the skin design, as well as the thickness of the members, which influences the overall stiffness of the design. The publication will present a workflow, in which the rotor is being structurally designed coming all the way from a generic CAD model, considering cg location as well as elastic deformation of the elastic skin and calculating the cross section wise stiffness of structure. This section wise approach is followed by the setup of a beam model of the blade for dynamic analysis as well as the setup of a 3D model for strength analysis as well as aeroelastic simulation by fluid structure interaction (FSI), the first results of which are shown as an example.

This is followed by a performance calculation in order to evaluate the efficiency of the concept and to provide input for further iteration steps. This includes trim analyzes for various blade loading conditions in hover as well as various forward flight velocities using DLR comprehensive analysis code S4. Chord-extension of up to 100% and chord-extension-deflection of up to 15deg are considered. Results show that the linearly variable chord-extension concept is effective in reducing power requirement in both hover and forward flight. The chord-extension-deflection helps reduce power requirement in hover, especially at higher blade loadings.

Keywords: morphing, rotor, helicopter, trailing edge, chord extension

NOTATION

BL	Baseline
cg	Center of gravity
CFRP	Carbon fiber reinforced polymer
EPDM	Ethen-Propen-Dien-Monomer
FM	Rotor Figure of Merit
FSI	Fluid structure interaction
GFRP	Glass-fibre reinforced plastic
CL	Lift coefficient
c	Rotor blade chord length, m
CT	Rotor thrust coefficient
EI_η	Flap stiffness, Nm²
EI_ζ	Lag stiffness, Nm²
f	Rotor natural frequency in Hz

FEA	Finite-Elemente-Analyse
GJ	Torsional stiffness, Nm²
m’	Mass per unit, kg/m
P	Required rotor power, kW
r	Rotor blade radius variable, m
R	Radius of rotor, m
sc	Shear center
X_{CG}	Chordwise location, center of gravity of Airfoil, m
X_{SC}	Chordwise location, shear center of Airfoil, m
μ	Advance ratio
σ	Rotor solidity
θ0	Rotor collective angle, deg
ω	Rotor natural frequency, rad/s
Ω	Rotor rotational speed, rad/s
Ω_{ref}	Reference rotor rotational speed, 44.4 rad/s

I. Introduction

Helicopters are characterized by their ability to control both the hover and the fast forward flight. This results in a wide range of capabilities. An important role is played by the design of the rotor blades, which always represents a compromise between fast forward flight and hovering flight. This results in a fixed rotor blade geometry that does not work optimally in either flight condition. A morphing rotor blade, which is able to change its shape during flight and thus optimally adapt its design parameters to the respective condition, can compensate for this disadvantage.

The topic of the morphing rotor blade has been moving more and more into focus in recent times. In Ref. 1, several morphing concepts were examined for their ability to improve helicopter performance in cruise flight. These include variable blade radius, variable blade chord length and variable rotor angular speed. The variable blade chord length was found to be a very effective morphing parameter for increasing rotor performance in cruise flight. In the Ref. 2 and 3, it was shown that the morphing of the chord extension over a section in span direction can reduce the power demand of the main rotor in stall-dominant flight conditions, while being able to increase the maximum gross weight, flight altitude and flight speed of the aircraft.

Within the European research program SABRE, several morphing concepts are being investigated, all of which aim to increase the performance of the helicopter. Within the SABRE project, DLR is responsible for the analysis and development of the concept of variable chord expansion. In this paper a structural concept is presented which can enable a helicopter rotor blade to change its chord length. A numerical review of the efficiency of the concept follows.

II. Structural Design of Flexible Trailing Edge

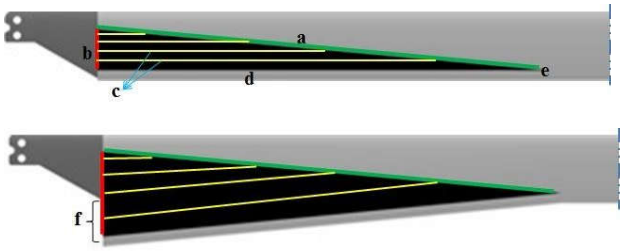

Figure 1. Unmorphed rotor blade (top) and the fully extended rotor blade a) auxiliary spar (green), b) guidance system (red), c) web stiffeners, d) rear spar, e) hinge, f) maximum chord-extension

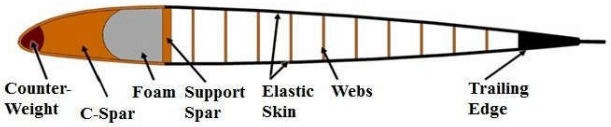

Figure 2. Blade cross-section

A rear spar is located in the trailing edge and can be swept back around a pivot point, which is located at 60% blade radius. At the innermost radial location of the aerodynamic profile (at 22% blade radius) this spar is actuated perpendicular to the radial direction by an actuator. In this region the blade consists of a conventional front structure, made of a conventional C-spar, a counterweight and a conventional load bearing composite skin. This conventional region ends at a diagonally implemented auxiliary spar, which is the starting point for the morphing rear part of the blade. In this rear part, an elastic skin is used, which allows the morphing to take place. Unidirectional reinforcements in the radial direction account for the centrifugal loads on the skin. In order to maintain the blade shape of the soft skin, a number of support elements are used. They keep the distance between the upper and lower skin and transfer aerodynamic loads from the skin into the auxiliary spar and a support at the root. The trailing edge rear spar is carried out as a stiff component which transfers the actuator force applied at the blade root and transmits the deflection all the way up to the pivot point. The described concept is shown in Figure 2. Below are the main characteristics summarized.

1. chordmorphing through elastic skin
2. rear spar in the trailing edge
3. swept back around a pivot point (joint)
4. actuator at the innermost radial location
5. conventional front structure (C-spar, counterweight and conventional load bearing composite skin)
6. morphing area starts from the diagonally auxiliary spar

7. reinforcing fibers in the skin carry centrifugal loads of the skin
8. webs maintain the blade shape of the elastic skin

For the blade design an optimization routine has been established which is able to calculate the blade properties. The routine is based on a section wise analysis of the rotor blade. For the design of the concept, 8 different cross sections were defined between 22% and 60% radial position, whose results were interpolated for the entire morphing range.

The optimization routine starts with a model generator in which all design variables are stored parametrically. The FE tool imports the surfaces and volumes of the CAD model and discretizes them for the calculation. Subsequently, the layer structure was defined for the individual components of the concept. In a first loop, the center of gravity of the model is determined and the counterweight is varied until the center of gravity reaches the c / 4-line. In a second loop, the calculation of the inertia moments, mass properties, as well as the calculation of the stiffnesses takes place. The result of this loop are the rotor bladeproperties, such as the positions of the individual axes (center of gravity, shearcenter, tension center) and stiffnesses. These values can then be used to calculate the blade dynamics and stability analysis. This process is visualized in Fig. 3.

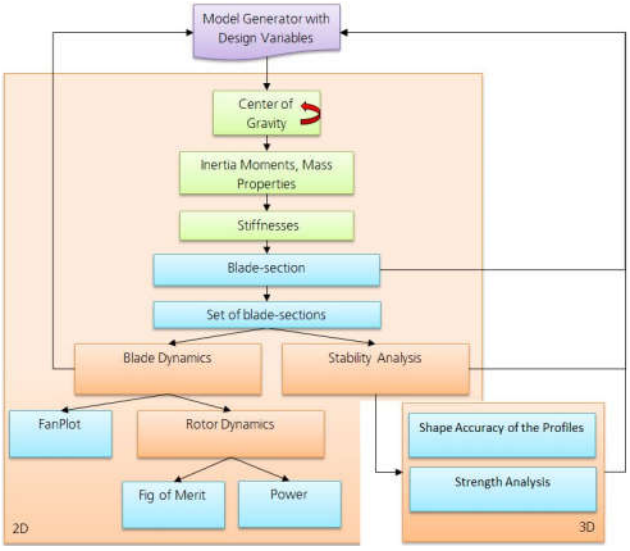

Fig. 3. Process of the optimization routine

To evaluate the shape accuracy of the profiles two different approaches are used. One is a local approach, which is looking at the wrinkling of the skin due to the pressure on the outside at a given substructure. The main task here is to find a suitable compromise between a low in plane stiffness of the elastic material, for a better actuation and a low out of plane deformation due to the aerodynamic loads. The in plane stiffness thus defines the size and thus weight of the required actuator. The out-of-plane deflection of the skin changes the surface of the profile, which has a negative effect on the aerodynamic properties.

For the concept presented, the elastic skin is stretched by over 160% with a 100% chord extension. Here, a thin sheet of EPDM material, between 0.5mm and 1.5mm is used, which allows strains up to 800%. Likewise, the use of a pre-stressed skin was considered. However, this resulted in a significant increase in out of plain displacement with increasing elongation. Therefore, the prestressing is kept as small as possible, which in turn has a positive effect on the required actuator force and the material fatigue of the skin itself.

FE analysis of the skin behaviour under pressure as a function of the web distance and the skin thickness was carried out at constant ambient pressure of 13 kPa. Results of this study can be seen in Fig. 4. Two morphing states were examined for this analysis: fast-forward (chord extension 0%) and hover (chord extension 100%). Fig. 5 shows one example result of skin deflection with varying web spacing and different skin thicknesses.

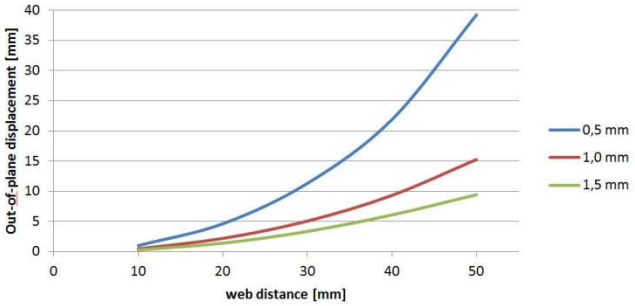

Fig. 4. Out of plane deflections over web distance for skins with different skin thickness.

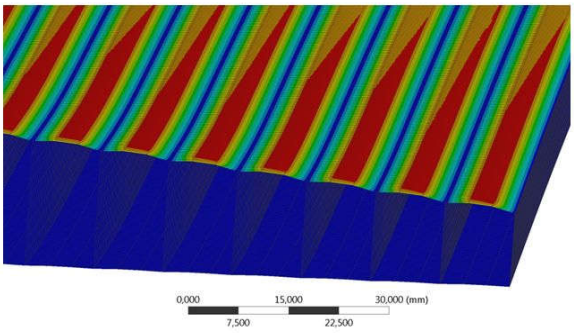

Fig. 5. FEA result of the skin out of plane deflection due to pressure loading for web distance of 10 mm.

On top of this investigation on the local effects of the skin, there was also an approach to look at the overall deflections of the structure in an aeroelastic coupling. The substitution of the rigid skin and the foam core, a conventional rotor blade, by an elastic skin with discrete points of support, results in a significant loss of rigidity of the trailing edge. The aerodynamic loads have to be derived from webs stored at two points in the auxiliary spar and the guide in the root area. The

resulting out-of-plane displacement lead to a non-negligible change in the shape of the airfoil. This changes the resulting pressure distribution across the profile. In order to be able to map this changed load, the structural design process is supplemented by an iterative process, which comprises five steps:

1. Creation of structural model
2. Calculation of actuator-induced deflection in ANSYS
3. Calculation of pressure distribution of the deflected trailing edge in XFOIL
4. Calculation of the resulting deflection with aerodynamic pressures in ANSYS
5. Comparison and evaluation of deflected airfoil geometry

This was carried out for several different flight conditions: hover as well as fast forward flight. For fast forward flight, three azimuth positions were chosen for aerodynamic loading. It is assumed that the hover has identical aerodynamic boundary conditions in every position.

In a CAD program, the blade structure was created as a shell model. The model itself is in turn parameterized so that changes can be automated within the scope of a sensitivity study or optimization. In contrast to the previously presented optimization routine (Fig. 3), a 3D model is now used, which includes all components of the concept. In Ansys followed the discretization of the model. Furthermore, the material properties and the layer structure of the individual components were defined here. Two models were provided by CAD for the simulation. First, an unmorphed model for the fast forward flight, which corresponds to the normal rotor blade profile, but has a modified, internal structure. The second model corresponds to the fully morphed rotor blade with a chord deflection of 100% at 22% radial position, for hovering. These two models are unloaded and represent the reference profiles for the pressure calculation. For the aerodynamic pressure distribution, XFOIL was used. 8 different profile cross sections in the span direction between 22% and 60% radius were determined to calculate the pressure distributions of both models. From the individual pressure distributions, a global pressure field was interpolated, which represents the starting conditions for the FE simulation. For the coupling, new cross sections are extracted from the deformed blade and a new pressure calculation in X-FOIL is carried out. This process can be repeated until the displacement of the trailing edge converges. Normally three to four iterations were required until the changes were kept at 1%. This process is visualized in Fig. 6.

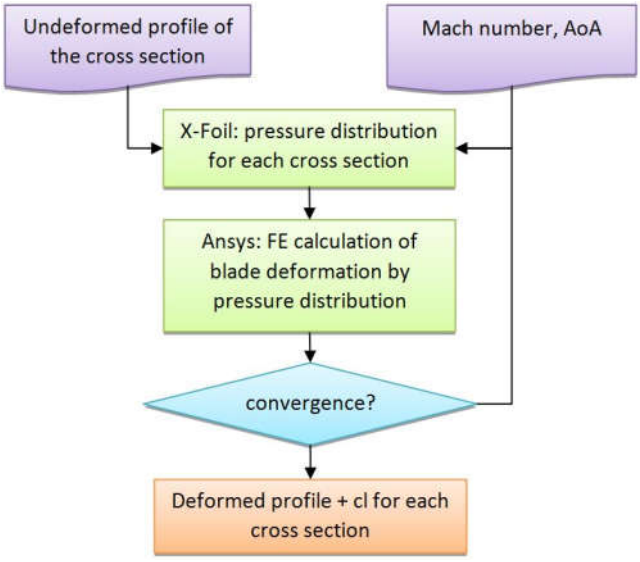

Fig. 6. Flowchart of the aero-structural coupled simulation

The results of the aerodynamic coupling show a deficit in the current design and the trailing edge stiffness, which is penalized with a reduction of the lift coefficients. This effect is particularly dominant in fast forward flight (Fig. 8), where the largest aerodynamic loads occur. By modifying the material properties, however, this effect can be weakened. At moderate loads, such as those found in hover (Fig. 9), the reduction in the lift coefficient is much lower. But here, too, additional reinforcements have a positive effect.

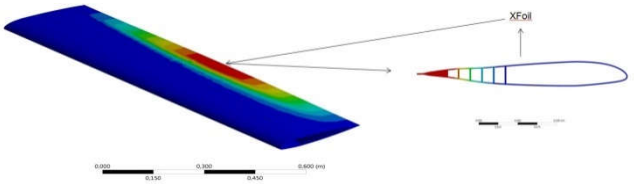

Fig. 7. Aeroelastic Coupling

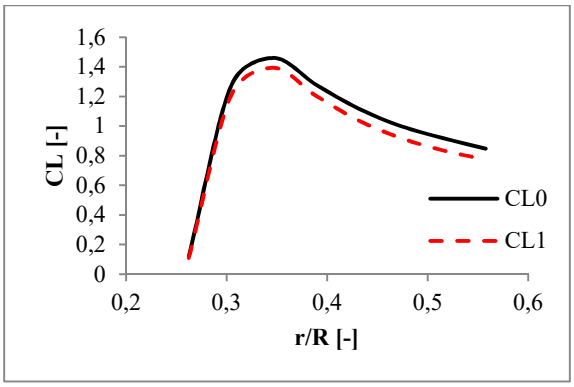

Fig. 8. Lift coefficients for fast forward flight at 180° azimuth position in span direction: CL0 - rigid blade, CL1- elastic blade with FSI

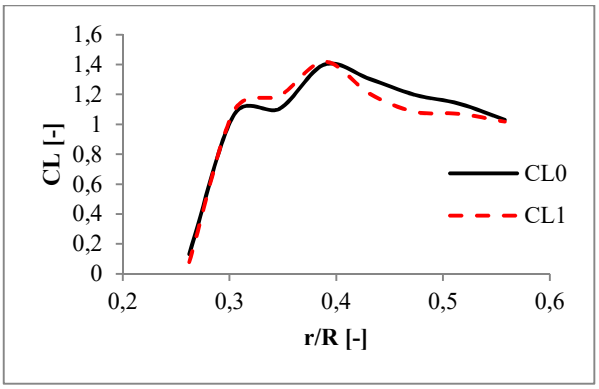

Fig. 9. Lift coefficients for hover flight in span direction: CL0 - rigid blade, CL1- elastic blade with FSI

A. Structural dynamics

The results of the rotor bladeproperties calculations are shown for a given hinge position of 0.6R in Fig. 10 for discrete chord extensions. They are compared to the unchanged Bo105 rotor blade, which serves as a base rotor. The area modified by the concept is between 22% R and 60% R. The 0% chord-extension rotor is most aerodynamically consistent with the baseline profile. Only the discretely supported, elastic skin differs from the base profile by a slight polygon formation. Further differences result from the additional auxiliary spar, the substructure and the elastic skin, which changes the mass and stiffness distributions in the morphed area. By substituting the hard foam filler in the baseline blade, through a light substructure of web stiffeners, as well as the glass fiber fabric skin in the morphing area, through light elastic skin, the mass density, m '(Fig. 10 a) and flap stiffness distribution, EI_{η} (Fig. 10 b) for the 0% chord extension blade are not significantly different from those of the baseline blade. With increasing chord extension, these properties change only slightly. The concept has a greater influence on the lag bending stiffness EI_{ζ}; (Fig. 10 c) and the torsional stiffness GJ (Fig. 10 d) distribution. The difference between the concept and the baseline rotor blade at the hinge position can be explained by a changed material choice for the conservative front part of the profile. Here, the GFRP was replaced by stiffer CFRP. Again, there is only a slight change in properties depending on chord extension. In Fig. 11, the locations of the shear centers (a) and center of gravity (b) with respect to the leading edge in terms of the baseline chord length for the discrete points defined in the optimization are shown in the spanwise direction. In this case the baseline rotor is compared with discrete chord extension. For the baseline blade, the shear center is ahead of the quarter-chord line, and the center of gravity coincides with the quarter-chord line. In the extended-chord cases, the shear center and the center of gravity are further away from the leading edge in the inboard sections as the mass moves farther from the leading edge. These values approach the quarter-chord as the section approaches the hinge. Since in the first loop the optimization is only performed by the 0% rotor, only its cg is on the c / 4 line. An enlargement of the chord extension leads to an enlargement of the gyration radius.

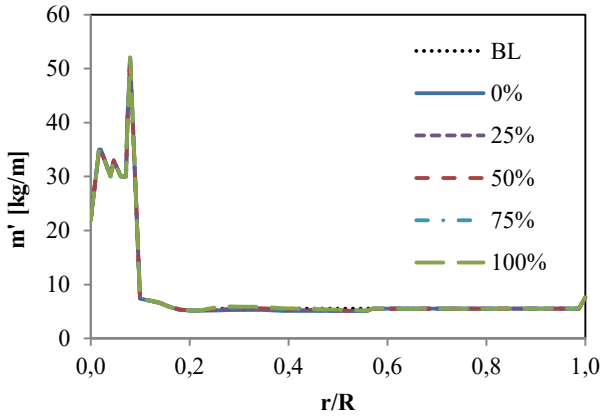

a) Radial distribution of mass per unit length

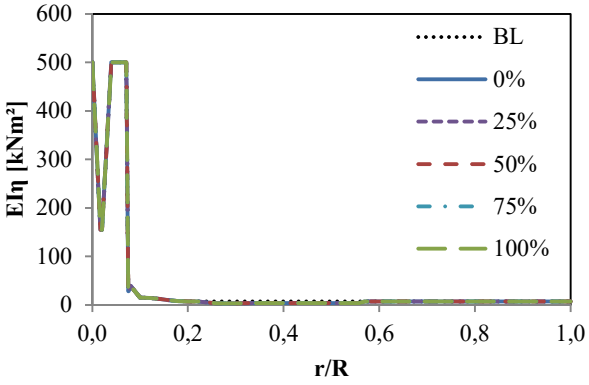

b) Flap stiffness radial distribution

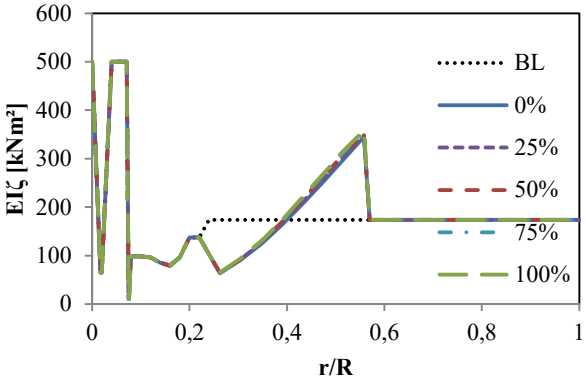

c) Lag stiffness radial distribution

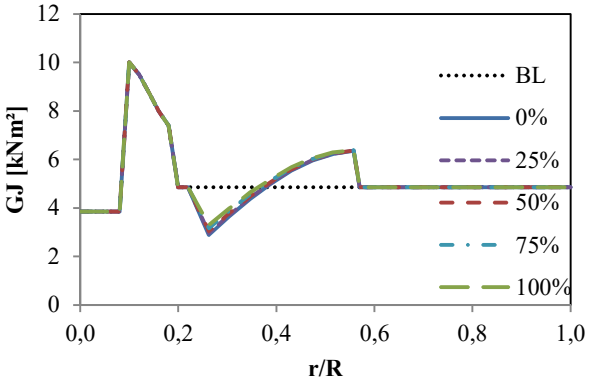

d) Torsion stiffness radial distribution

Fig. 10. Structural data distribution of the baseline and chord-extended rotor blades

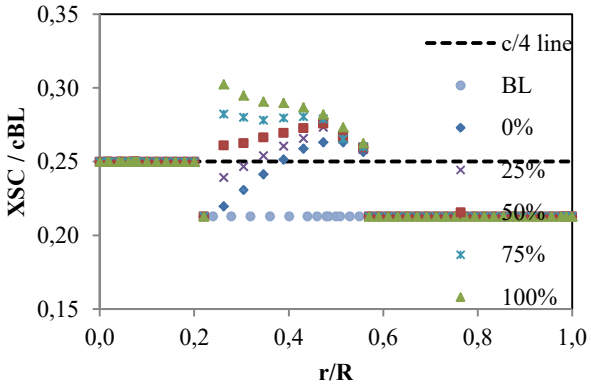

a) Shear center

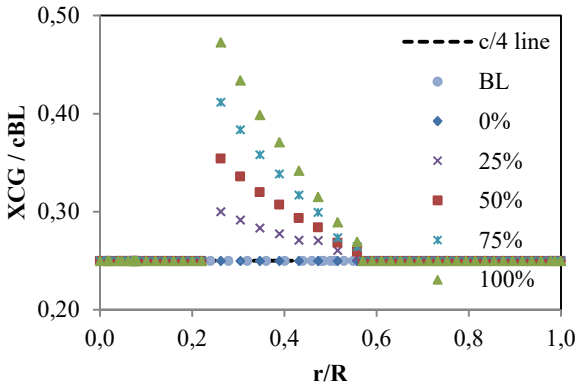

b) Center of gravity

Fig. 11. Shear center (X_{sc}), center of gravity (X_{cg}) radial variation as a ratio of the baseline chord

III. RESULTS OF THE PERFORMANCE CALCULATION

The structural data of the different surrogate models are used to perform structural dynamic analysis and obtain the Campbell diagram. Fig. 12 compares the Campbell diagram of the baseline rotor blade with those of 0%, 25%, 50% and 100% chord-extension cases. The diagrams show the first few natural modes until 10/rev. The fundamental flap and lag mode have hardly been affected. In line with the structural properties distribution, the higher flap frequencies have slightly reduced for the 0% chord-extension compared to the baseline rotor but there isn't much variation with increase in the chord-extension percentage. Flap-torsion coupling is seen close to the operating rotor speed for the chord-extension cases. However, it isn't critical. This coupling is due to the offset of center of gravity from the shear center. The second lag mode has slightly increased for the morphed rotors while the third lag mode reduces to below 10/rev. The torsional frequencies are the most affected and have reduced considerably. The first torsion mode decreases with increasing chord-extension. The second torsion mode reduces to below 10/rev for the morphed rotor. This reduction in torsional frequencies is, mostly, due to the increasing offset of the center of gravity from the shear center as the maximum chord-extension is increased.

A. Trim analysis

Isolated rotor trim analysis is then performed on the morphed rotor cases and their power requirements are compared with those of the baseline rotor. The baseline rotor geometrical and operating parameters are given in Table 1 in the Appendix. Trim analysis is carried out for hover for up to a baseline blade loading (C_T/σ_{BL}) of 0.16 and for forward flight velocities from 0 m/s to 70 m/s (μ = 0.32). The target hub moments are taken to be zero. Both chord-extension and chord-extension-deflection are considered.

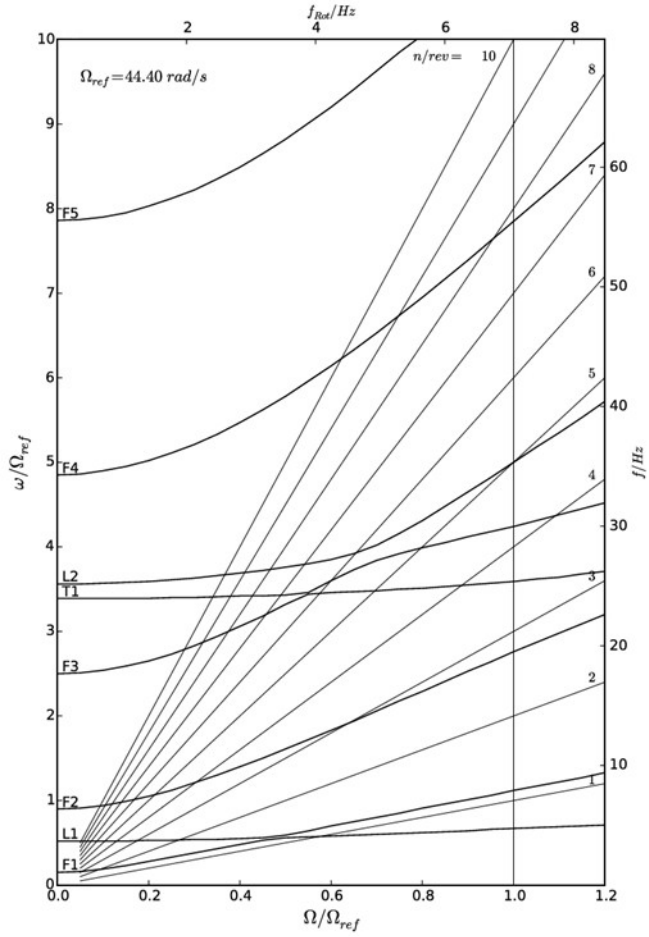

a) 0% maximum chord-extension rotor

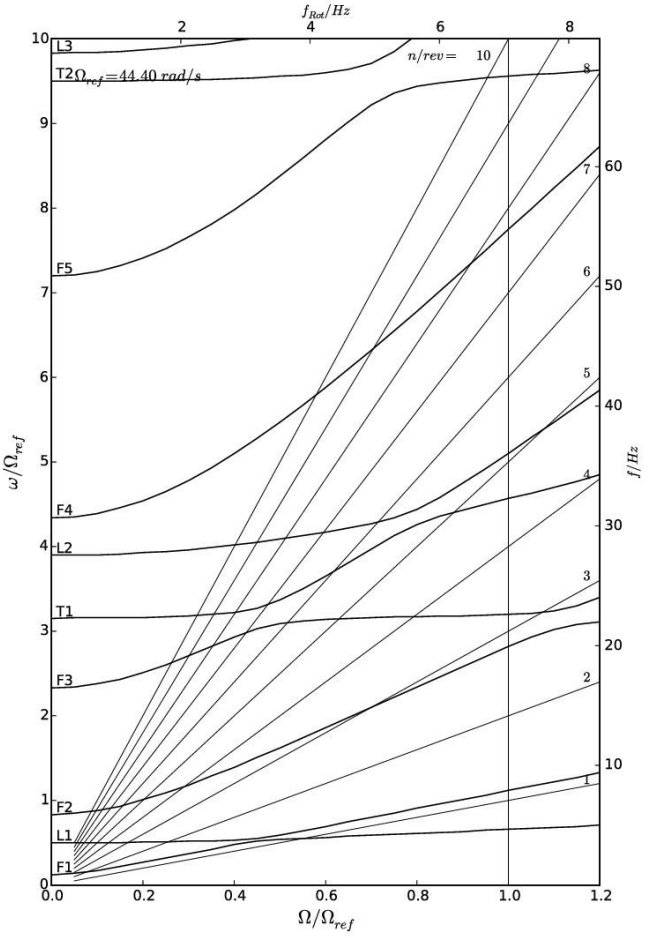

b) 25% maximum chord-extension rotor

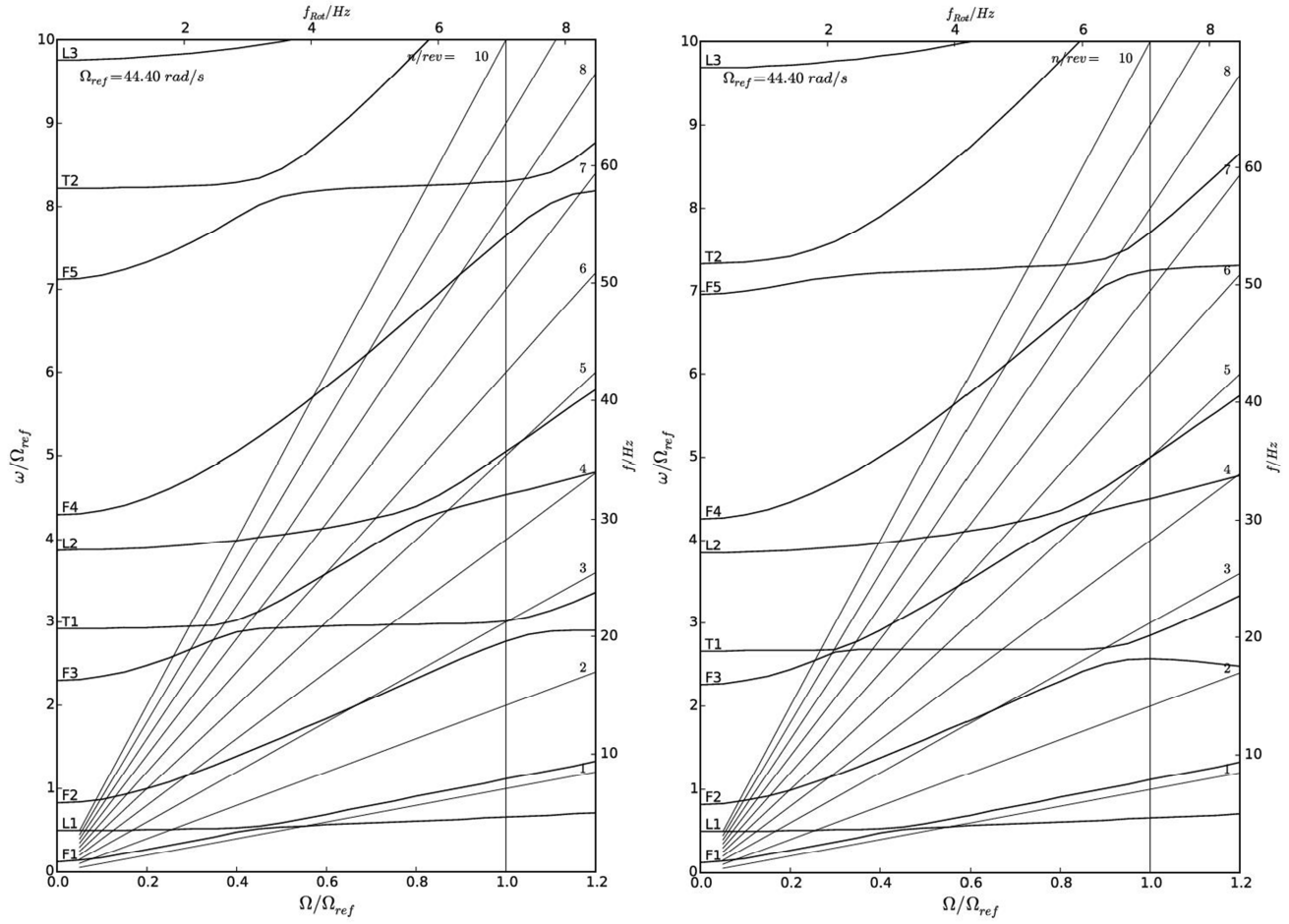

c) 50% maximum chord-extension rotor

d) 100% maximum chord-extension rotor

Fig. 12. Campbell diagrams for baseline and morphed rotors

B. Variation of blade loading at hover

Fig. 13a shows the figure of merit variation with baseline blade loading for various chord-extension cases. The design blade loading for the baseline Bo105 rotor is $C_T/\sigma_{BL} = 0.0714$. It is clearly seen that the figure of merit (FM) increases with increase in chord-extension. The FM for the baseline rotor at design thrust is 0.65. For the same thrust, the FM for 100% chord-extension is 0.7 representing an increase of 5 counts. The maximum FM of 0.73 is achieved for 100% chord-extension for $C_T/\sigma_{BL} = 0.1$. Fig. 13b shows the collective angle variation with blade loading for baseline and chord-extended rotors. It can be seen that for a particular thrust, the collective angle requirement increases with increase in the chord-extension. For $C_T/\sigma_{BL} = 0.0714$, the required collective angle is 7.7 deg while for 100% chord-extension case, the required collective angle increases by 3.6 deg to 11.3 deg. Similarly, at $C_T/\sigma_{BL} = 0.16$, the required collective angle increases to 17.6 deg for the 100% chord-extension case from 13 deg for the baseline rotor. The increase in the collective angle requirement is accompanied by a decrease in the tip elastic twist of the blade as can be seen from Fig. 14 which shows the elastic twist for the different blades at $C_T/\sigma_{BL} = 0.16$. Elastic twist which was nose-up for the baseline rotor decreases in magnitude and turns negative (nose-down) as chord-extension increases.

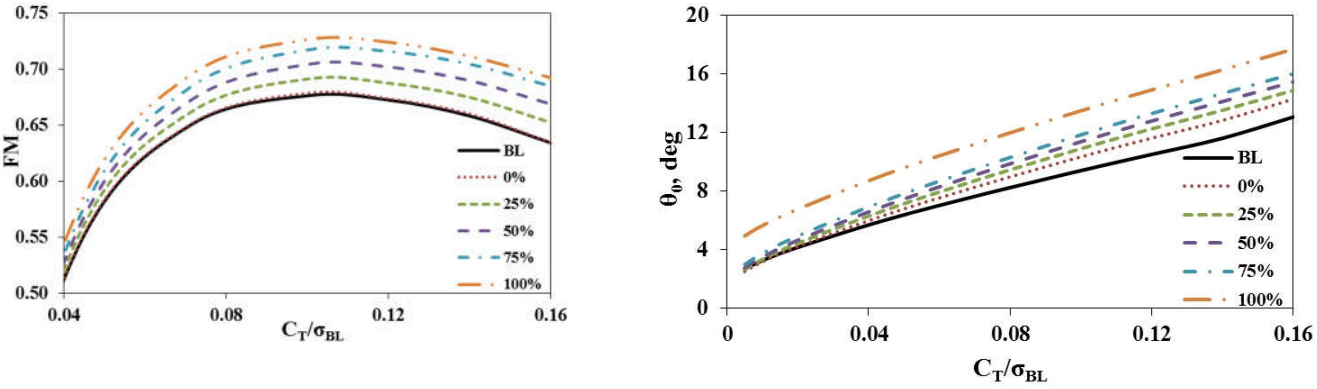

a) FM variation with blade loading

b) Collective angle variation with blade

Fig. 13. Figure of merit variation with blade loading for baseline and chord-extension rotors

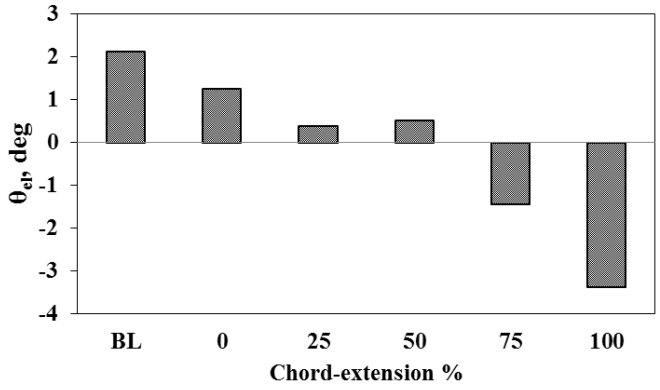

Fig. 14. Elastic torsion at CT/σBL = 0.16

C. Variation of advance ratio at C_T/σ_{BL} = 0.0714

Fig. 15 shows the variation of rotor required power with advance ratio for the baseline rotor and rotors with varying chord-extension. It is seen from the plot that the required power reduces with increase in chord-extension, especially at lower velocities. At hover, there is a drop of about 25kW for the 100% chord-extension case relative to the baseline rotor. At μ = 0.1, this drop reduces to 14kW. At higher velocities, the chord-extended rotors give mixed results for required power when compared to the baseline rotor. The 0% chord-extension rotor requires less power than the baseline rotor while the 100% chord-extension rotor requires more power. However, it is to be noted that the 100% chord- extension case was found to be difficult to trim at high velocities and the results presented here need to be taken with higher tolerance. The actual power required may be lower at high advance ratios.

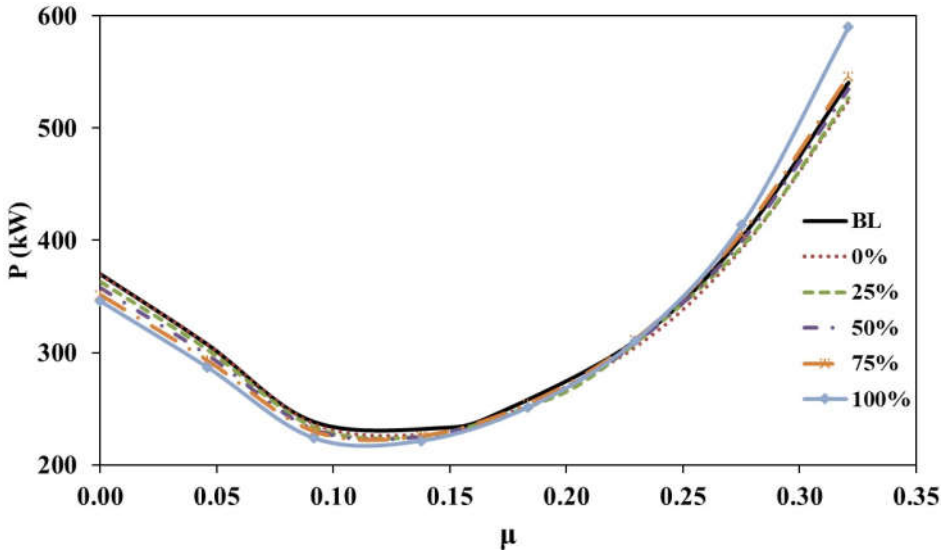

Fig. 15. Rotor required power variation with advance ratio for different maximum chord-extensions

IV. CONCLUDING REMARKS

This paper shows a concept for the structural realization of a chord morphing and how it is currently being implemented. This includes a simulation framework for the structural design as well as the results of some structural and aeroelastic analysis. Considered was a rotor blade with a maximum chord extension of 100%, which decreases in the direction of the blade tip. The performance calculation generated on this basis showed promising potential for improving the efficiency of a helicopter. At the moment she is neglecting the aeroelastic coupling.

ACKNOWLEDGMENT

This work was funded by the European Research Council (ERC) under the European Union's Horizon 2020 research and innovation programme, as part of the Shape Adaptive Blades for Rotorcraft Efficiency (SABRE) programme (grant agreement No 723491).

APPENDIX

Table 1. Table 1. Baseline rotor parameters

Description	Symbol	Value	Unit
Radius	R	4.912	m
Angular Velocity	Ω	44.4	rad/s
Blade chord	c	0.27	m
Number of blades	N_b	4	-
Rotor solidity	σ	0.07	-
Precone angle (pos. upward)	β_0	2.5	deg
Pitch-flap coupling	Δ_3	0	deg
Radius of blade attachment main bolt	r_{att}	0.372	m
Root cutout	rc	1.1	m
Linear twist of airfoiled section	Θ_{tw}	-8	deg/R
Effective blade mass	m_b	24.2	kg
Lock number (sea level)	γ	8.1	-
Fundamental flap frequency	γ_β	1.117	-
Fundamental lag frequency	γ_ζ	0.666	-
Fundamental torsion frequency	γ_θ	3.59	-

REFERENCES

1. KANG, H., SABERI, H., AND GANDHI, F., "DYNAMIC BLADE SHAPE FOR IMPROVED HELICOPTER ROTOR PERFORMANCE," JOURNAL OF THE AMERICAN HELICOPTER SOCIETY, VOL. 55, (3), JULY 2010, PP. 32008

2. KHOSHLAHJEH, M., AND GANDHI, F., "EXTENDABLE CHORD ROTORS FOR HELICOPTER ENVELOPE EXPANSION AND PERFORMANCE IMPROVEMENT," JOURNAL OF THE AMERICAN HELICOPTER SOCIETY, VOL. 59, (1), JAN. 2014, PP. 1-10.

3. BARBARINO, S., GANDHI, F., AND WEBSTER, S. D., "DESIGN OF EXTENDABLE CHORD SECTIONS FOR MORPHING HELICOPTER ROTOR BLADES," ASME 2010 CONFERENCE ON SMART MATERIALS, ADAPTIVE STRUCTURES AND INTELLIGENT SYSTEMS, AMERICAN SOCIETY OF MECHANICAL ENGINEERS, JAN. 2010, PP. 323-336.